In: Energy Technology 2026, 15-19 March 2026, San Diego, USA, The Minerals, Metals & Materials Series, pp. 147-159
DOI: 10.1007/978-3-032-13909-2_14

Comparative Life Cycle Assessment of WTaTiVCr High-Entropy Alloy Fabricated by Mechanical Alloying and 3D Mixing Methods

Jiarui Feng[1], Emanuele Pagone*[1], Owais Ahmed Waseem[2]

[1]*Sustainable Manufacturing Systems Centre, Faculty of Engineering and Applied Sciences, Cranfield University, Cranfield, Bedfordshire, MK43 0AL, United Kingdom*

[2]*Research and Development, Aurubis Richmond, GA 30906, USA*

* Corresponding Author. Email: e.pagone@cranfield.ac.uk

Abstract

WTaTiVCr High-Entropy Alloys (HEAs) are recognized as promising candidates for fusion plasma-facing applications. However, the environmental impact of their development and fabrication methods remains insufficiently characterized. This study presents a comparative evaluation of two powder processing routes: mechanical alloying by ball milling and low-shear 3D mixing. Both fabrication methods yield single-phase, Body-Centred Cubic WTaTiVCr HEAs with comparable Vickers hardness and relative densities exceeding 98%. Applying a "cradle-to-gate" (i.e. from raw material production to arc plasma sintering) Life Cycle Assessment method, the carbon footprint of both routes is estimated to produce the divertor surface of the International Thermonuclear Experimental Reactor. The findings identify the more environmentally friendly route as well as carbon footprint "hotspots". Results for the alloy with 90% of tungsten molar content, show a carbon footprint reduction of 75.8 tCO_2e, when switching from the ball milling to the 3D mixing manufacturing route. Such difference grows by a further 35% when the tungsten content increases up to 90% molar fraction.

Keywords

High-Entropy Alloy, Sustainability, Extraction and Processing, Fusion Plasma-Facing Materials

1. Introduction

While the development of advanced materials progresses toward extreme-environment applications, the sustainability of their manufacturing processes has become a growing concern. Among these materials, High Entropy Alloys (HEAs) such as W_xTaTiVCr have attracted considerable interest for their mechanical properties and radiation resistance, making them promising candidates for fusion reactor applications [1]. However, while their physical performance is well-documented [2], the environmental consequences of HEAs fabrication remain inadequately quantified, particularly in the context of embodied energy and carbon footprint.

HEAs based on refractory metals such as tungsten (W), tantalum (Ta), titanium (Ti), vanadium (V), and chromium (Cr), have gained traction for use in fusion reactors due to their high melting points, phase stability, irradiation resistance, and temperature-dependent yield strength at ambient and cryogenic conditions [3,4]. The work of Miracle and Senkov (2017) outline the fundamental design strategies of HEAs, emphasizing the potential of equiatomic and near-equiatomic compositions for tailoring mechanical and functional properties [5]. More specifically, Waseem and Ryu's study [6] demonstrate the feasibility of producing W_xTaTiVCr HEA through powder metallurgy, including mechanical alloying and Spark Plasma Sintering (SPS), highlighting the mechanical robustness and homogeneity of the resultant microstructure. Earlier work by Waseem and Ryu (in 2020) developed $W_{0.5}$TaTiVCr-based composites reinforced with a tungsten mesh, showing significant improvements in ductility and fracture toughness, further supporting their potential for fusion applications [7]. In addition, Alvi, Waseem, and Akhtar report that the SPS $W_{0.5}(TaTiVCr)_{0.5}$ alloy maintains a stable Body-Centred Cubic (BCC) structure up to 1400 ℃ with high strength and wear resistance,

making it suitable for plasma-surface materials, rocket nozzles and industrial molds applications [8]. Furthermore, $W_{0.5}(TaTiVCr)_{0.5}$ shows superior irradiation resistance compared to pure tungsten, under high-energy F^{3+} ion implantation, with smooth surface profiles and lower irradiation-induced strain [9]. Moreover, helium ion irradiation behavior of $W_{0.5}(TaTiVCr)_{0.5}$ shows only slight irradiation-induced damage and moderate hardening [10]. Because of the harsh operating environment in fusion reactors, low activation HEAs hold strong potential as divertor materials, like the surface of the Outer Vertical Target (OVT) in the International Thermonuclear Experimental Reactor (ITER), where plasma-facing components must endure extreme heat flux, irradiation, and mechanical stresses, while maintaining structural stability.

Previous research on mechanical alloying and elemental powder mixing has demonstrated the effectiveness of these methods in achieving homogeneous microstructures and improved mechanical properties for refractory HEAs such as TiTaVWCr or $W_xTaTiVCr$ [11,12]. However, neither study explicitly considered environmental impact indicators, such as carbon footprint or embodied energy, in the assessment of their fabrication. Although studies have advanced the understanding of microstructure and mechanical performance, they are unable to quantify environmental trade-offs. Quantifying environmental indicators is important because alternative manufacturing routes often involve highly energy-intensive and resource-demanding steps, which directly affect the embodied energy and carbon footprint of materials. Without such quantification, it is difficult to judge whether the mechanical advantages of a given route are worth its environmental cost. Although the number of publications on HEA production is increasing, relatively few studies have systematically assessed the environmental sustainability of different manufacturing routes. Liu *et al*. emphasized the need to include environmental indicators such as embodied energy and carbon footprint in evaluating advanced manufacturing methods [13]. This study quantitatively compares two powder mixing methods (3D mixing and ball milling), to produce WTaTiVCr HEAs, focussing on embodied energy and carbon footprint of a specific product with a "cradle-to-gate" (i.e. from raw material production to arc plasma sintering) Life Cycle Assessment (LCA) approach. It aims to fill the existing gap in HEA research, promoting the integration of life cycle thinking into materials engineering and advanced manufacturing [14]. The main objectives of this study comprise conducting route process mapping (identifying key manufacturing steps), collecting environmental impact data and building process models to compare embodied energy and carbon footprint for a representative component.

2. Materials and Methods

2.1 Raw Material, Powder Production and Product Mass

Raw material quantities necessary to produce non-equimolar $W_xTaTiVCr$ HEAs are calculated considering the variable molar ratios of tungsten (Table 1) of previous work by Waseem and Ryu [11]. Therefore, molar fractions x_i are converted into mass fractions w_i first obtaining the molar mass of each element m_i from molecular weights M_i

$$m_i = x_i\, M_i \tag{1}$$

next, determining the total mass m_t by summing the contributions of all elements

$$m_t = \sum(x_i\, M_i) \tag{2}$$

and finally calculating the mass fractions w_i (Table 2) dividing each molar mass by the total mass

$$w_i = \frac{x_i\, M_i}{m_t} \tag{3}$$

Relevant mixed powder densities ρ_{mix} (Table 2) are then calculated from mass fractions w_i and elemental densities ρ_i

$$\rho_{mix} = \frac{1}{\sum \frac{w_i}{\rho_i}} = \frac{1}{\frac{w_W}{\rho_W} + \frac{w_{Ti}}{\rho_{Ti}} + \frac{w_{Ta}}{\rho_{Ta}} + \frac{w_{Cr}}{\rho_{Cr}} + \frac{w_V}{\rho_V}} \tag{4}$$

Raw materials are assumed to be sourced in the following countries [16]: W: China, Ti: China, V: China, Ta: Congo, Cr: South Africa. Metal powder is assumed to be produced from ingots by Elementum 3D Ltd., and the relevant environmental impact data of ingot production and powder production are based on the Ansys Granta Selector database [15] and the work by Ehmsen *et al.* [15].

Table 1. Nominal formula of $W_xTaTiVCr$ high-entropy alloys studied by Waseem and Ryu [11] to be assessed.

	Tungsten Molar fraction	Nominal alloy formula
HEA	30%W	$W_{0.3}(TaTiCrV)_{0.7}$
HEA Derivatives	40%W	$W_{0.4}(TaTiCrV)_{0.6}$
	50%W	$W_{0.5}(TaTiCrV)_{0.5}$
	60%W	$W_{0.6}(TaTiCrV)_{0.4}$
	70%W	$W_{0.7}(TaTiCrV)_{0.3}$
	80%W	$W_{0.8}(TaTiCrV)_{0.2}$
	90%W	$W_{0.9}(TaTiCrV)_{0.1}$

Table 2. Mass fraction w_i of each $W_xTaTiVCr$ high-entropy alloy element and relevant mixed powder density ρ_{mix} as a function of tungsten molar fraction x_{W}.

x_{W}	w_{W}	w_{Ta}	w_{Ti}	w_{Cr}	w_{V}	ρ_{mix} (kg/m^3)
0.300	0.487	0.280	0.074	0.080	0.079	12118.99
0.400	0.596	0.220	0.058	0.063	0.062	13162.11
0.500	0.689	0.170	0.045	0.049	0.048	14199.40
0.600	0.769	0.126	0.033	0.036	0.036	15230.90
0.700	0.838	0.088	0.023	0.025	0.025	16256.66
0.800	0.899	0.055	0.015	0.016	0.016	17276.74
0.900	0.952	0.026	0.007	0.008	0.007	18291.17

The product considered in this study is the divertor surface of ITER that comprises approximately 200 000 tungsten armour units (Figure 1a), each measuring $12 \times 28 \times 28$ mm (Fig 1c) [17,18]. Such units include a tube width, an inner diameter of 12 mm and a wall thickness of 1.5 mm, an interlayer thickness of 1 mm, and the facing side thickness of 8 mm (Figure 1c) [18,19], yielding to volume of 6.684×10^{-6} m^3. Therefore, the overall volume to cover the entire divertor surface is about 1.3368 m^3.

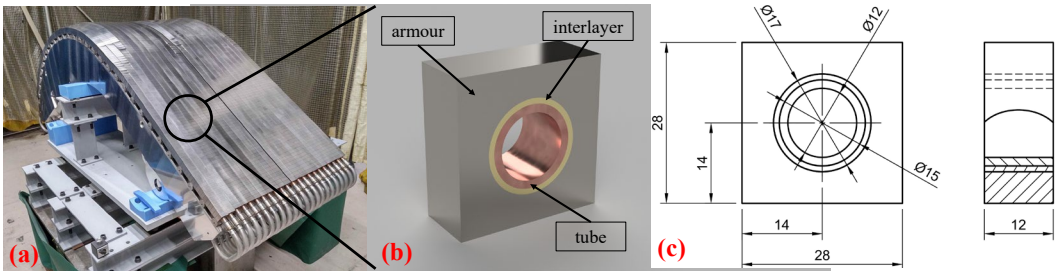

Figure 1. (a) Divertor of ITER. (b) Single block of OVTs on the divertor inner surface. (c) Technical drawing of single OVT for ITER (Unit: mm).

2.2 Mixing, Spark Plasma Sintering and Transportation lifecycle steps

The 3D mixing and high-energy ball milling manufacturing routes have been mapped in process steps (Figure 2) where the only difference is the powder preparation method. Both routes begin with the extraction and refinement of raw materials (W, V, Cr, Ta, Ti), followed by transportation by air freight, truck, and ferry. Then the ingots of elemental raw materials are transformed into powder, after which mixing is carried out either via 3D mixing or by high-energy milling. SPS produces the final product. The use phase and the end of life of the product (e.g. disposal, recycling, …) are out of scope for this study.

The equipment considered for the mixing processes are the TURBULA 3D Shaker Mixer T2C (3 hours of mixing time at 30 rpm of rotational speed [7]) for 3D mixing and the Retsch Drum Mill TM 300 (24 hours of processing at 300 rpm of rotational speed [11,12]) for ball milling. The SPS was modelled considering Dr. Sinter SPS-212LX with a sintering temperature of 1600 °C under vacuum atmosphere (10^{-3} Torr ≈ 0.133 Pa) and 50 MPa die pressure with the heating rate is 100 °C/min [11].

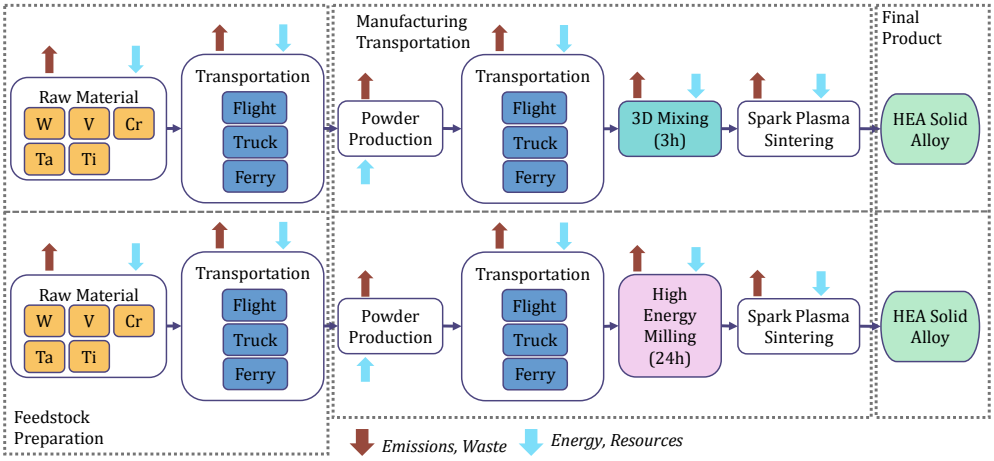

Figure 2. Cradle-to-Gate process flow diagram for HEA production via 3D mixing and High-Energy ball milling routes.

Transportation emissions were estimated adding 5% packaging weight to the cargo and considering a combination of Euro 4, 16-32 tons truck and a bulk carrier.

2.3 Mixing Process Material Efficiency Calculation

Material losses during the mixing process caused by adhesion of the powder on the container walls are estimated with the Johnson-Kendall-Roberts (JKR) contact mechanics model [20]. Such model is particularly suitable for analysing the adhesive behaviour of high surface energy materials, such as micro-sized tungsten or titanium powders, when they come into contact with rigid container surfaces. The solid-vapor surface energy γ_{SV} of tungsten range between 2.77 J/m^2 at the melting temperature to 3.25 J/m^2 (at 0 K) [21], thus at room temperature $\gamma_{SV} \approx 3.1\ J/m^2$ [21]. For clean homogeneous contact, the work of adhesion $W = 2\gamma_{SV}$ [22]. Applying the JKR model, the magnitude of the pull force F_{pull} can be estimated considering also the powder particle effective radius R [20]. Powder particle sizes used match the work by Waseem and Ryu [11]: Tungsten (W) = 1.21 µm, Vanadium (V) <75 µm, Chromium (Cr) = 63 µm, Tantalum (Ta) <45 µm, and Titanium (Ti) = 45 µm.

$$F_{pull} = \left(\frac{3}{2}\right)\pi\, R\, W \tag{5}$$

Considering also the density of the powder particle ρ, the mass of the particle m_p is

$$m_p = \left(\frac{4}{3}\right)\pi R^3 \rho \tag{6}$$

the gravitational force magnitude F_g reads

$$F_g = m_p g = \left(\frac{4}{3}\right)\pi R^3 \rho g \tag{7}$$

If $\frac{F_{pull}}{F_g} >> 1$ the powder adhesion force exceeds the gravitational force. According to Newton's Second Law, the critical detachment acceleration a_{crit} is

$$a_{crit} = \frac{F_{pull}}{m_p} = \frac{9\,W}{8\,(\rho R^2)} \tag{8}$$

The zero load contact radius a_0 and Tabor parameter μ (used to select the JKR regime) could be calculated with Equations (9) and (10) considering the elastic modulus E^* and the separation distance between powder particles and the container surface at equilibrium z_0

$$a_0 = \left[\frac{(6\pi R^2 W)}{E^*}\right]^{\frac{1}{3}} \tag{9}$$

$$\mu = \left(\frac{R \cdot W^2}{E^{*2} {z_0}^3}\right)^{\frac{1}{3}} \tag{10}$$

If $\mu > 5$ the JKR model is suitable [23] and the JKR model can be used to estimate the amount of powder that could adhere to the container surface. Under the assumption of the BCC crystal structure, each particle occupies a minimum repeating unit volume that can be expressed in 2D by the repeating unit area A_{cell}

$$A_{cell} = (2R)^2 = 4R^2 \tag{11}$$

Accordingly, the theoretical maximum density of particles per unit area $N_{\max}$ and mass of single particles m_p could be calculated by Equation (12) and (6).

$$N_{\max} = \frac{1}{A_{cell}} = \frac{1}{(4R^2)} \tag{12}$$

According to the calculation result, the maximum monolayer surface mass density σ_{max} could be calculated

$$\sigma_{max} = N_{max}\, m_p = \frac{1}{4R^2}\rho\left(\frac{4}{3}\right)\pi R^3 = \frac{\pi\rho R}{3} \tag{13}$$

In practical applications σ_{max} derived from ideal close-packing configurations often overestimates the actual surface coverage due to irregular particle arrangements, surface roughness, or spreading imperfections. To account for these deviations, a coverage factor $f \in [0,1]$ is introduced, yielding an engineering-corrected residual mass density. Typically, for static resting: $f \sim 0.1$, after normal discharge: $f \sim 0.01$, with intensive cleaning: $f \leq 10^{-3}$.

$$\sigma = f\,\sigma_{max} \tag{14}$$

To calculate the material efficiency of the mixing process the inner surface area and volume could be calculated as follows:

$$A_{total} = 2\pi RH + 2\pi R^2 \tag{15}$$

$$V_{total} = \pi R^2 H \tag{16}$$

Assuming a packing density coefficient $\eta = 60\%$ as randomly packed spherical micro-sized powders, and for 40% Volume Filling. The density of HEA powder could be calculated by Equation (17).

$$\rho_{powder} = \eta\,\rho W \tag{17}$$

Then the material efficiency E_m can be calculated

$$E_m = \frac{m_{total} - m_{waste}}{m_{total}} \times 100\% = \frac{\rho_{powder} V_{total\times 0.4} - A_{total}\times\sigma}{\rho_{powder} V_{total\times 0.4}} \times 100\% \tag{18}$$

3. Results

Estimating the material efficiency of the two powder mixing processes using the method in Section 2.3, the 3D mixing process shows to be characterised by negligible losses, whereas they are measurable for ball milling (Table 3).

Table 3. Input data used to apply the method in Section 2.3 and corresponding material efficiency E_m. R: powder particle effective radius, ρ_{mix}: mixed powder density, σ_{max}: maximum monolayer surface mass density.

HEA Type	R (m)	ρ_{mix} (kg/m^3)	σ_{max} (kg/m^2) 3D Mixing	σ_{max} (kg/m^2) Ball Milling	E_m (%) 3D Mixing	E_m (%) Ball Milling
30%W	1.88×10^{-6}	12118.99	2.39×10^{-5}	2.52×10^{-5}	99.999967	99.738746
40%W	1.44×10^{-6}	13162.11	1.98×10^{-5}	2.12×10^{-5}	99.999975	99.974858
50%W	1.17×10^{-6}	14199.40	1.74×10^{-5}	1.87×10^{-5}	99.999980	99.979610
60%W	9.83×10^{-6}	15230.90	1.57×10^{-5}	1.71×10^{-5}	99.999983	99.982836
70%W	8.49×10^{-6}	16256.66	1.45×10^{-5}	1.59×10^{-5}	99.999985	99.985169
80%W	7.48×10^{-6}	17276.74	1.35×10^{-5}	1.51×10^{-5}	99.999987	99.986935
90%W	6.69×10^{-6}	18291.17	1.28×10^{-5}	1.44×10^{-5}	99.999988	99.988319

The consequent cradle-to-gate carbon footprint *CFP* and embodied energy E_e grow, through both manufacturing routes, together with the tungsten molar fraction of the alloy (i.e. from 30% to 90%), because tungsten production is more resource intensive than the other elements in the alloy. Computing the difference in *CFP* and E_e between the ball milling and the 3D mixing routes (ΔCFP and ΔE_e, Fig 3) for the entire ITER divertor surface, the difference is significant. Specifically, at 30% tungsten molar fraction, the *CFP* of the 3D mixing route is 48.76 tCO_2e lower, whereas at 90% tungsten molar fraction such reduction is 75.8 tCO_2e. Considering the cumulative energy consumption, the reduction in switching from ball milling to 3D mixing ranges between 160 (with 30% W) and 340 GJ (with 90% W). Therefore, 3D mixing demonstrates better environmental performance across all compositions.

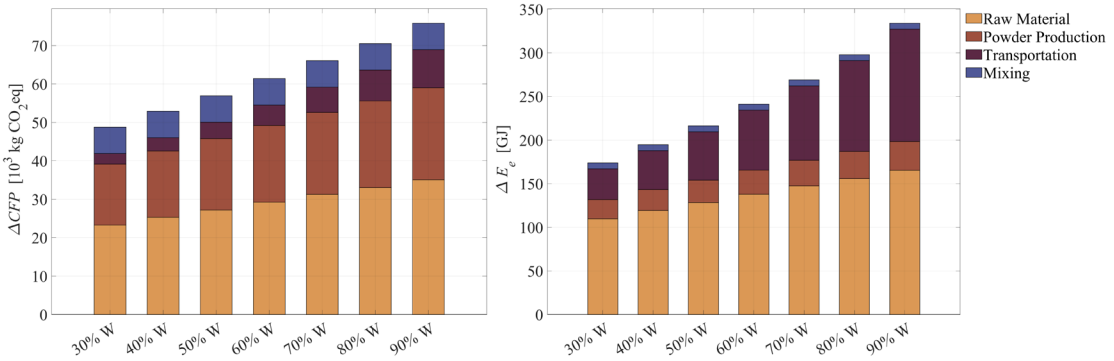

Figure 3. Contributions of production steps to the carbon footprint difference (ΔCFP) and embodied energy difference (ΔE_e) between the ball milling route and the 3D mixing route (see Fig. 2) for High Entropy Alloys with different tungsten molar fractions in percentage points (%W).

Table 5. Typical exploited ore grade of different tungsten molar fraction.

HEA Type (tungsten molar fraction)	Typical exploited ore grade (%)
30% W	4.81
40% W	4.14
50% W	3.58
60% W	3.1
70% W	2.68
80% W	2.32

The main contributor of ΔCFP and ΔE_e is the production and smelting of tungsten from ore. Furthermore, as the tungsten content increases, the change in transportation-related *CFP* becomes more significant than that from ore production and smelting. The main reason is that tungsten has a relatively low typical exploited ore grade (economically viable metal content in mined ores) ranging between 1.62% and 1.79% [15]. Typical exploited ore grade for different tungsten compositions in the HEA are reported in Table 5. A lower ore grade means that more raw mineral material is required, which leads to higher *CFP* from transportation. Increasing the molar tungsten content from 30% to 90%, the typical exploited ore grade decreases by 2.49%, while the transportation-related *CFP* difference increases by 264%. Similar considerations can be made regarding the energy consumption. Although the differences in *CFP* and E_e from transportation and ore production increase with the tungsten content, the difference in the mixing stage does not grow in the same way. Finally, in the sintering step, the quantity of the input material and process parameters are the same for both routes, making it irrelevant in the comparative analysis (i.e. not yielding any difference between routes of ΔCFP and ΔE_e).

4. Conclusion

This study shows that, in the production of tungsten-based HEA powders, 3D mixing provides better environmental sustainability than ball milling, specifically in terms of *CFP* and E_e. Based on a cradle-to-gate

LCA, a 3D mixing production route results in lower environmental impact at different tungsten content levels. Producing the ITER divertor surface with a tungsten-based HEA through 3D mixing, its *CFP* can be reduced by as much as 75.8 tCO_2e, when compared with production by ball milling. Similarly, E_e can be reduced as much as 340 GJ. Such differences stem from the superior material efficiency of the mixing stage that requires a lower demand of raw material up the supply chain. By contrast, ball milling may provide better particle uniformity and compatibility with traditional systems, but its higher energy use and carbon emissions put it at a disadvantage in sustainability terms.

The shown environmental advantage of the 3D mixing route provides not only a significant scientific finding, but also a practical reference for the metal powder manufacturing industry that have limited visibility of the environmental consequences up their supply chain. The principles highlighted by the results of this study can be applied more generically to the environmental assessment of HEAs, an aspect often under considered.

Based on these findings, it is recommended that industry bodies and policymakers include 3D mixing in the green process catalogue for powder metallurgy processes. It should be promoted especially in critical stages such as advanced alloy preparation and batch mixing. In parallel, environmental certification systems based on life cycle indicators should be introduced to standardize equipment efficiency, energy sources, and emissions, thereby improving transparency and regulatory compliance across the manufacturing chain.

Future work could broaden the scope of assessment to include more environmental factors, such as land use, water stress, and air pollution, to develop a more comprehensive sustainability assessment. Exploration into renewable energy sources, bio-based additives, and intelligent mixing strategies is also encouraged to further enhance environmental performance. Additionally, it is advised to develop dynamic LCA models for mixing processes that can adapt to real-world variations in production, such as different batch sizes, delivery times, and logistics routes. This would support low-carbon decision-making in complex supply chain scenarios.

5. References

[1] Wang X, He H, Jie S, Hai-Yan X, Da-Qiao M (2021) Recent progress of tungsten-based high-entropy alloys in nuclear fusion. *Tungsten* 3(2):143–160. https://doi.org/10.1007/s42864-021-00089-9

[2] Barron PJ, Carruthers AW, Fellowes JW, Pickering EJ, Jons NG, Dawson H (2020) Towards V-based high-entropy alloys for nuclear fusion applications. *Scripta Materialia* 176:12–16. https://doi.org/10.1016/j.scriptamat.2019.10.043

[3] Senkov ON, Wilks GB, Miracle DB, Chuang CP, Liaw PK (2010) Refractory high-entropy alloys. *Intermetallics* 18(9):1758–1765. https://doi.org/10.1016/j.intermet.2010.05.014

[4] Gludovatz B, Hohenwarter A, Catoor D, Chang EH, George EP, Ritchie RO (2014) A fracture-resistant high-entropy alloy for cryogenic applications. *Science* 345(6201):1153–1158. https://doi.org/10.1126/science.1254581

[5] Miracle DB, Senkov ON (2017) A critical review of high entropy alloys and related concepts. *Acta Materialia* 122:448–511. https://doi.org/10.1016/j.actamat.2016.08.081

[6] Zhang Y, Xie M, Wang Z, Song X, Mu R, Gao J, Bao J, Zhou F, Pan W (2023) Unveiling the underlying mechanism of unusual thermal conductivity behavior in multicomponent high-entropy (La0.2Gd0.2Y0.2Yb0.2Er0.2)2(Zr1–Ce)2O7 ceramics. *Journal of Alloys and Compounds* 958:170471. https://doi.org/10.1016/j.jallcom.2023.170471

[7] Waseem OA, Ho JR (2020) W0.5TaTiVCr-based composite reinforced with W-mesh for fusion plasma-facing applications. *Functional Composites and Structures* 10.1088/2631-6331/ab7980. https://dx.doi.org/10.1088/2631-6331/ab7980

[8] Sajid A, Waseem OA, Farid A (2020) High Temperature Performance of Spark Plasma Sintered W0.5(TaTiVCr)0.5 Alloy. *Metals* 10.3390/met10111512. https://dx.doi.org/10.3390/met10111512

[9] Waseem OA, Woller KB, Sweidan FB, Ryu HJ (2020) Effects of F3+ ion implantation on the properties of W and W0. 5 (TaTiVCr) 0.5 for depth marker-based plasma erosion analysis. *Nuclear Materials and Energy* 10.1016/j.nme.2020.100806. https://doi.org/10.1016/j.nme.2020.100806

[10] Waseem OA, Ryu HJ (2021) Helium ions irradiation analysis of W0. 5 (TaTiVCr) 0.5 for application as a future fusion plasma-facing material. *Materials Chemistry and Physics* 0.1016/j.matchemphys.2020.124198. https://doi.org/10.1016/j.matchemphys.2020.124198

[11] Waseem OA, Ryu HJ (2017) Powder metallurgy processing of a WxTaTiVCr high-entropy alloy and its derivative alloys for fusion material applications. *Scientific Reports* 7:1926. https://doi.org/10.1038/s41598-017-02035-2
[12] Sutrisna, Prasetiyo AB, Kartikasari R, Aziz I (2023) Effect of milling time variation on TiTaVWCr HEA powder as nuclear material on microstructure and mechanical properties by a mechanical alloying method. *IOP Conf. Ser.: Earth Environ. Sci.* 1151:012052. https://doi.org/10.1088/1755-1315/1151/1/012052
[13] Wickramasinghe KC, Sasahara H, Suda S (2020) Green metalworking fluids for sustainable machining applications: A review. *Journal of Cleaner Production* 257:120552. https://doi.org/10.1016/j.jclepro.2020.120552
[14] Allwood JM, Ashby MF, Gutowski TG, Worrell E (2012) *Sustainable Materials: With Both Eyes Open*. UIT Cambridge Ltd, Cambridge, UK. ISBN: 9781906860059
[15] Ansys (2024) *Granta Selector 2024: Sustainability Database (Advanced Level3)*. Ansys, Cambridge, UK.
[16] Ehmsen S, Conrads J, Klar M, Aurich JC. (2025) Environmental impact of powder production for additive manufacturing: Carbon footprint and cumulative energy demand of gas atomization. *Journal of Manufacturing Systems* 82:13–25. https://doi.org/10.1016/j.jmsy.2024.11.004
[17] Hirai T, Panayotis S, Barabash V, Amzallag C, Escourbiac F, Durocher A, Merola M, Linke J, Loewenhoff Th, Pintsuk G, Wirtz M, Uytdenhouwen I (2016) Use of tungsten material for the ITER divertor. *Nuclear Materials and Energy* 9:616–622. https://doi.org/10.1016/j.nme.2016.04.012
[18] Ezato K, Suzuki S, Seki Y, Hirayama T, Yamada H, Escourbiac F, Hirai T (2018) Development of tungsten divertor components for ITER in Japan. *Fusion Engineering and Design* 136:683–689. https://doi.org/10.1016/j.fusengdes.2018.03.020
[19] El-Morshedy SE-D (2024) Thermal-hydraulic simulation of ITER tungsten divertor monoblock for loss of flow transient. *Nuclear Materials and Energy* 38:101616. https://doi.org/10.1016/j.nme.2024.101616
[20] Johnson KL, Kendall K, Roberts AD (1971) Surface energy and the contact of elastic solids. *Proc R Soc Lond A* 324(1558):301–313. https://doi.org/10.1098/rspa.1971.0141
[21] Tyson WR, Miller WA (1977) Surface free energies of solid metals: Estimation from liquid surface tension measurements. *Surface Science* 62(1):267–276. https://doi.org/10.1016/0039-6028(77)90442-3
[22] Ebnesajjad S (2014) *Surface Tension and Its Measurement*. Elsevier, Oxford, pp. 7–24. ISBN: 9780323265632
[23] Maugis D (1992) Adhesion of spheres: the JKR-DMT transition using a Dugdale model. *Journal of Colloid and Interface Science* 150(1):243–269. https://doi.org/10.1016/0021-9797(92)90285-T

Comparative life cycle assessment of WTaTiVCr high-entropy alloy fabricated by mechanical alloying and 3D mixing methods

Feng, Jiarui

2026-03-19

Feng J, Pagone E, Waseem OA. (2026) Comparative life cycle assessment of WTaTiVCr high-entropy alloy fabricated by mechanical alloying and 3D mixing methods. In: Energy Technology 2026, 15-19 March 2026, San Diego, USA, The Minerals, Metals & Materials Series, pp. 147-159

https://doi.org/10.1007/978-3-032-13909-2_14